J. Fluid Mech. (2024), *vol*. 988, A45, doi:10.1017/jfm.2024.403

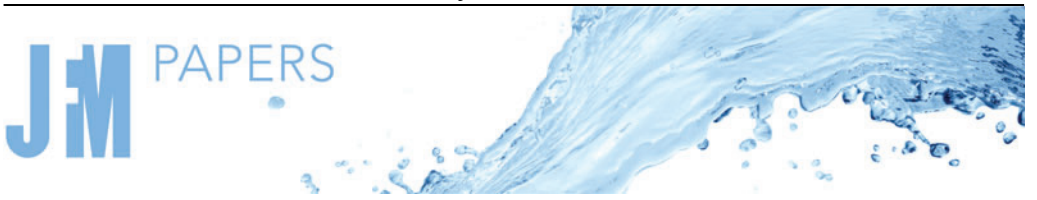

One-dimensional analysis of pressure variations induced by trains passing each other in a tunnel

Tokuzo Miyachi[1],†, **Yuhei Noguchi**[1] **and Yuki Yamauchi**[1]

[1]Railway Technical Research Institute, 2-8-38 Hikari-cho, Kokubunji-shi, Tokyo 185-8540, Japan

(Received 18 March 2023; revised 27 March 2024; accepted 13 April 2024)

In this study, the asymptotic solutions of the pressure variations induced by two trains passing each other in a tunnel are theoretically investigated. The one-dimensional inviscid compressible airflow is analysed, and two methods to obtain numerically exact solutions and M_H expansion formulas for approximate equations are presented, where M_H is the Mach number of the high-speed train. The pressure coefficient, corresponding to the maximum value of the magnitude of the pressure, is expressed as $|c_p|_{max} = |c_{p,min}| = [(R/(1-R))(1+\alpha)^2 + (R(1-R)/(1-2R)^2)(1-\alpha)^2] + O[M_H]$, where $c_{p,min} < 0$, $\alpha = U_L/U_H$ and U_L and U_H denote the speeds of the low- and high-speed trains, respectively, and R is the cross-sectional area ratio of the train to the tunnel. The theoretical results indicate the dependence of the speeds of the two trains on the pressure distribution and that the maximum magnitude of the asymptotic pressure for a fixed value of M_H is obtained for $\alpha = 1$ and $\alpha = 0$ when $R < R_c$ and $R > R_c$, respectively, where R_c denotes the critical blockage ratio. Because the airflow along the side of the low-speed train, induced by the low-speed train, is along the running direction of the high-speed train and reduces the relative velocity of the high-speed train as the two trains pass each other, $|c_p|_{max}$ for $\alpha = 0$ is larger than $|c_p|_{max}$ for $\alpha = 1$ when $R > R_c$. It is theoretically demonstrated that, as conventional high-speed railway systems satisfy $R < R_c$, a conservative pressure estimation can be established assuming $\alpha = 1$.

Key words: flow–structure interactions, shock waves, aeroacoustics

1. Introduction

In railway tunnels, pressure variations are induced by trains entering, passing through and leaving tunnels (Tollmien 1927; Yamamoto 1974; Vardy 1976; Woods & Pope 1981; Glöckle & Pfretzschner 1988; Gawthorpe 2000; Baron, Mossi & Sibilla 2001; Saito, Iida & Kajiyama 2011). The magnitudes of these variations significantly impact passenger comfort, train stability, car body fatigue and infrastructure (Kobayashi *et al.* 1998; Sima

† Email address for correspondence: miyachi.tokuzo.06@rtri.or.jp

2003; Qian *et al.* 2019). Thus, estimating the magnitudes of pressure variations in high-speed railway tunnels is important and should be considered in railway system design, for instance, when determining the required structural strengths and allowable train speed limits.

Trains passing through a tunnel introduce transient pressure variations (Fujii & Ogawa 1995; Howe 2000; Hwang *et al.* 2001; Gilbert, Baker & Quinn 2013; Chu *et al.* 2014; Li *et al.* 2017; Liu *et al.* 2017; Liu, Jing & Ren 2018; Lu *et al.* 2019); in particular, a train entering and leaving a tunnel generates pressure waves (Hara 1961; Sugimoto & Ogawa 1998; Howe *et al.* 2006). The pressure magnitude in a double-track tunnel is at its maximum when the pressure variations generated by two trains passing each other and the pressure wave generated by a train entering or leaving the tunnel superpose. Therefore, numerous studies have addressed this phenomenon. However, research on two trains passing each other in a tunnel remains limited compared with that on the generation of pressure waves when a train enters or leaves a tunnel. This could be attributed to the difficulty in performing model experiments of two trains passing each other. Although moving model rigs have considerably contributed to experimental studies, most of these rigs can only launch one train model, except in special facilities (Yang, Song & Yang 2016). Therefore, researchers have generally performed only numerical studies in this context.

The Shinkansen line connecting the islands of Honshu (main) and Hokkaido in Japan has been operational since March 2016. A key component of this route is the Seikan tunnel, an undersea tunnel spanning 54 km. As high-speed trains (320 km h^{-1}) share the Seikan tunnel with conventional freight trains (110 km h^{-1}), the high-speed trains must run through the tunnel at a reduced speed of 160 km h^{-1}, except under special circumstances (Railway Gazette International 2021; Tsuru 2021). This mixed traffic scenario poses a novel challenge for Japanese railway systems, particularly because freight trains lack the streamlined and sealed design characteristic of high-speed trains. Consequently, allowing an increase in the speed limit for Shinkansen trains along the Seikan tunnel would require thorough investigation of several aerodynamic considerations specific to mixed traffic operations.

Generally, mixed traffic includes trains operating at two different speeds: high-speed trains (e.g. those with speeds over 160 km h^{-1}) and conventional trains (e.g. those with speeds less than 130 km h^{-1} in Japan). In emergencies, one train may run at a very low speed or remain stationary in a tunnel, even in non-mixed traffic scenarios (typical high-speed railway tunnels). Although numerous studies (Fujii & Ogawa 1995; Hwang *et al.* 2001; Chu *et al.* 2014; Li *et al.* 2017; Lu *et al.* 2019; Qian *et al.* 2019) have been conducted on the impact of train speed, train length, tunnel length and passing location when two trains pass each other travelling at the same speed, few investigations (Howe 2000; Liu *et al.* 2018) have considered the case of the trains running at different speeds. Available closed formulas for the maximum magnitude of the pressure wave generated by a train entering a tunnel (Hara 1961) or passing through a junction of the main tunnel and a branch (Miyachi, Fukuda & Saito 2014) are useful for structural design. In contrast, except for the closed formula for the pressure rise of pressure waves when two trains pass each other (Howe 2000), no analytical formulas are available to determine the pressure distribution around two trains passing each other at the same or different speeds inside a tunnel. In particular, we must evaluate the negative pressure in the region occupied by the two running trains because it is much greater than the magnitude of the pressure variation of the pressure waves generated by the two trains passing each other. In addition, the time waveforms of the difference in pressure between the nose and tail, the left and the right sides and the outside and inside of the trains are important because they are directly related

to passenger comfort, train fatigue, train stability while in operation and the safety of train freight.

Although the flow and pressure fields of trains passing each other are three-dimensional, viscous, transient and compressible, their main component corresponds to that of a one-dimensional inviscid flow. Additionally, because the use of three-dimensional computational fluid dynamics (CFD) is still costly, the initial engineering design of a railway tunnel system widely relies on the use of one-dimensional CFD tools (e.g. ThermoTun software (Vardy 1976; Dundee Tunnel Research 2023)). Therefore, theoretical formulas of asymptotic pressure solutions based on a one-dimensional flow analysis remain highly valuable for railway engineers. Thus far, theoretical investigations on the pressure field around two trains passing each other in a tunnel have not been conducted because solving the one-dimensional compressible flow equations under such conditions is difficult and assuming an incompressible flow is not applicable.

In this study, the pressure variation induced by two trains passing each other in a tunnel is theoretically analysed for $R < 0.35$, where R is the cross-sectional area ratio of the train to the tunnel. Quasi-one-dimensional (quasi-1-D) governing equations are introduced, and M expansion formulas of asymptotic pressure solutions are presented by simplifying the Hara method (Hara 1961), which is based on the perturbation method of pressure. The remainder of this paper is organized as follows: § 2 presents the results of a 1-D inviscid compressible airflow analysis. Section 3 interprets the results of two trains passing each other using approximate equations. Section 4 discusses the results reported in §§ 2 and 3. Finally, § 5 concludes the paper.

2. One-dimensional analysis of inviscid compressible airflows for two trains passing each other

2.1. *Train speeds and blockage ratios in Japanese railways*

The train speed U and blockage ratio R ($R = A_t/A_0$, where A_t and A_0 denote the cross-sectional areas of the train and tunnel, respectively) are key parameters for two trains passing each other. In Japan, the speeds of high-speed (Shinkansen) and conventional trains are less than 320 and 130 km h^{-1}, respectively. For typical Shinkansen trains, the blockage ratio is approximately 0.17 (less than 0.2). The blockage ratio of double-decker Shinkansen trains is approximately 0.22; however, their maximum speed is 240 km h^{-1}. The blockage ratio of conventional freight trains in a double-track tunnel is less than 0.25, and this ratio is expected to be less than 0.12 for maglev trains.

As the minimum cross-sectional area of the Seikan tunnel is the same as those of other Shinkansen tunnels, the blockage ratios for both Shinkansen and conventional freight trains are less than 0.2.

2.2. *Governing equations and exact solutions*

Figures 1 and 2 present the schematics of a high-speed train passing a low-speed train in a tunnel. The x-axis is set from left to right. The high- and low-speed trains, H and L, run at speeds of U_H and U_L in the negative and positive x-directions, respectively. The noses of two trains meet at $x = 0$ and $t = 0$, where t denotes time. To simplify the analysis, the blockage ratio and length of both trains are assumed to be equal. Stage A denotes the period after nose–nose passing but before nose–tail passing; stage B indicates the period after nose–tail passing but before tail–tail passing.

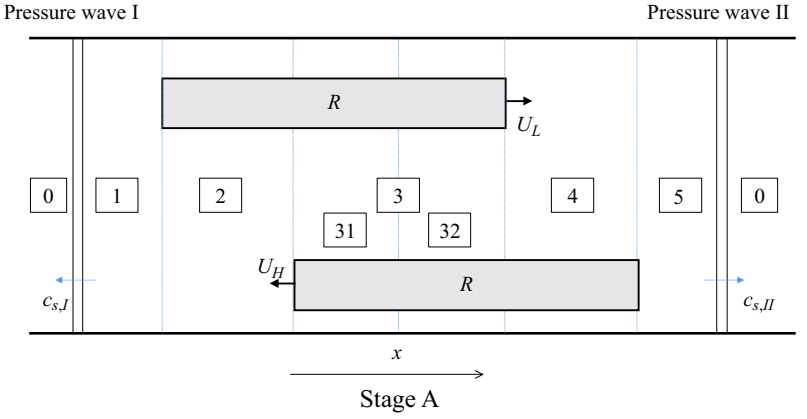

Figure 1. Schematic of two trains passing each other after nose–nose passing but before nose–tail passing.

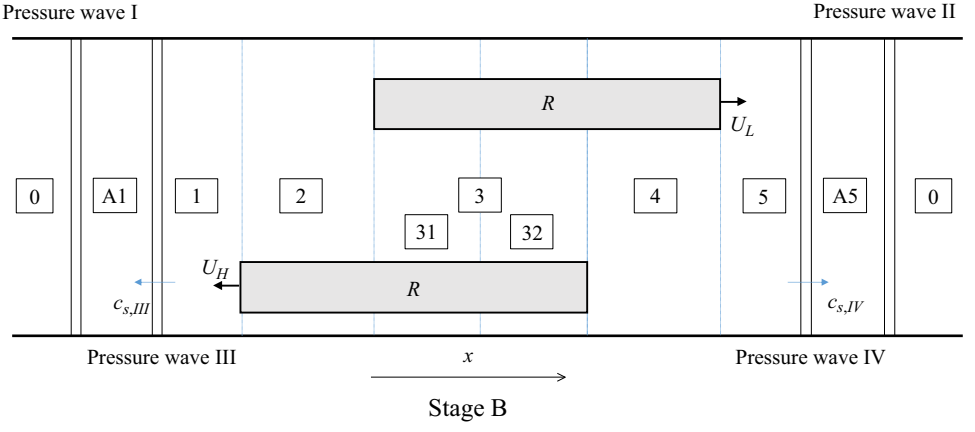

Figure 2. Schematic of two trains passing each other after nose–tail passing but before tail–tail passing.

In stage A, two pressure waves, denoted I and II, are considered at the fronts of the two trains. The area between the two waves is divided into six regions: 1, 2, 31, 32, 4 and 5. Region 3, which is occupied by the two running trains, consists of subregions 31 and 32. In region 0, the pressure and density are atmospheric, and the velocity is zero. In stage B, two additional pressure waves, denoted III and IV, are considered in front of each of the two trains, respectively. Regions A1 and A5 represent the states of regions 1 and 5 of stage A, respectively. The area between the two secondary waves is divided into six regions, as in stage A.

As pressure waves I and II are generated around the noses at the moment of nose–nose passing, they propagate through regions 2 and 4, respectively. When they depart from the train tails, the reflected waves return to the noses. In stages A and B, a steady state was assumed after multiple reflections of the waves at the noses and tails for simplicity.

For the following calculations, we assumed a 1-D inviscid compressible flow. In front of and behind each wave, three conservation laws (for continuity, momentum and energy) were adopted. For all other regions, two consecutive regions were connected using the continuity equation, energy equation and isentropic relationship with respect to a

coordinate system fixed on each train. For each wave, we have the following relations:

$$\rho_f^*(m_f - M_s) = \rho_b^*\,(m_b - M_s)\,, \tag{2.1}$$

$$X_f + \rho_f^*(m_f - M_s)^2 = X_b + \rho_b^*\,(m_b - M_s)^2\,, \tag{2.2}$$

$$\frac{\gamma}{\gamma-1}\frac{1/\gamma + X_f}{\rho_f^*} + \frac{1}{2}(m_f - M_s)^2 = \frac{\gamma}{\gamma-1}\frac{1/\gamma + X_b}{\rho_b^*} + \frac{1}{2}\,(m_b - M_s)^2\,, \tag{2.3}$$

where $\rho^* = \rho/\rho_0$ is the non-dimensional density, ρ is the density, ρ_0 is the atmospheric density, $X = p/(\gamma p_0)$ is the non-dimensional pressure, p is the acoustic pressure, p_0 is the atmospheric pressure, γ is the specific heat ratio, $m = u/c_0$ is the non-dimensional velocity, u is the air velocity, c_0 is the speed of sound, the subscript f indicates the state in front of a wave, the subscript b indicates the state behind a wave, $M_s = c_s/c_0$ and c_s is the speed of the acoustic wave (shock wave).

For the two consecutive regions, the continuity, Bernoulli and isentropic equations to be solved are for $i = 1, 2, 32, 4$

$$\rho_i^*(m_i - M_{ref})(1 - R_i) = \rho_{i+1}^*(m_{i+1} - M_{ref})(1 - R_{i+1}), \tag{2.4}$$

$$\frac{\gamma}{\gamma-1}\frac{1/\gamma + X_i}{\rho_i^*} + \frac{1}{2}(m_i - M_{ref})^2 = \frac{\gamma}{\gamma-1}\frac{1/\gamma + X_{i+1}}{\rho_{i+1}^*} + \frac{1}{2}(m_{i+1} - M_{ref})^2, \tag{2.5}$$

$$\frac{\rho_{i+1}^*}{\rho_i^*} = \left(\frac{1/\gamma + X_{i+1}}{1/\gamma + X_i}\right)^{1/\gamma}, \tag{2.6}$$

where $M_{ref} = U_{ref}/c_0$ is the Mach number of the reference train, U_{ref} is the reference train speed (U_H or U_L), $R_1 = R_5 = 0$, $R_2 = R_4 = R$, $R_3 = R_{31} = R_{32} = 2R$ and i is the index of the region.

The boundary between the subregions 31 and 32 is assumed to be a contact surface. As in $x < u_3 t$ and $x > u_3 t$, the airflows are induced by pressure waves I and II, respectively; they can have different density values. Therefore, we have the following continuity conditions for the velocity and pressure, whereas the densities in these two regions are different:

$$m_{31} = m_{32} = m_3, \tag{2.7}$$

$$X_{31} = X_{32} = X_3. \tag{2.8}$$

The application of (2.1)–(2.8) to regions 1–5 yields 20 variables and 20 equations. This implies that the systems of equations for stages A and B are fully ranked and solvable. It should be noted that flow analysis without pressure waves or a contact surface cannot be solved because the number of equations does not correspond with the number of variables. 'Python scipy.optimize.minimize' was used to solve (2.1)–(2.8). Although $R < 0.25$ in Japanese double-track tunnels, as outlined in § 2.1, this study considers the range of $0 \leq R \leq 0.35$. For this range, the calculation was stable when the initial guesses of X_i, m_i, $\rho^*/\rho_0 - 1$ and $M_s - 1$ were set to zero because flow choking did not occur. Figures 3–5 present the exact solutions for the pressure in each region, calculated using (2.1)–(2.8), where $\alpha = U_L/U_H$ is the ratio of the speeds of the trains. The difference between ρ_{31}^* and ρ_{32}^* was negligibly small when $X_i \ll 1$.

As shown in figures 3–5, the maximum magnitude of pressure is observed in region 3, when $\alpha = 1$ in stage A for $R = 0.2$ and when $\alpha = 0$ in stage B for $R = 0.3$. In addition, although the magnitudes of the pressure waves in regions 1 and 5 are almost zero for $U_H = 250\,\mathrm{km\,h^{-1}}$ and $R = 0.2$, they have increased (positive and negative) values for larger values of R or U_H.

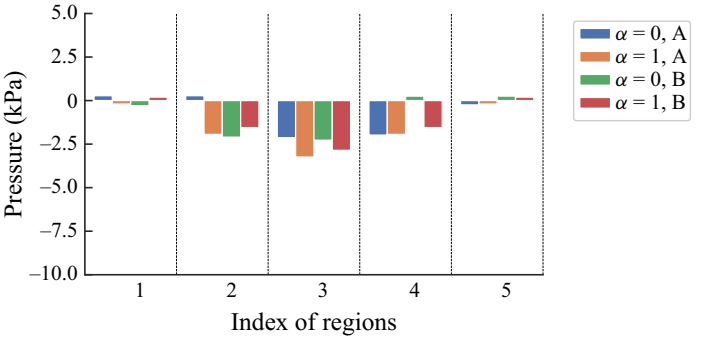

Figure 3. Exact solutions of the pressure distribution in each region: $U_H = 250\,\mathrm{km\,h^{-1}}$ and $R = 0.2$.

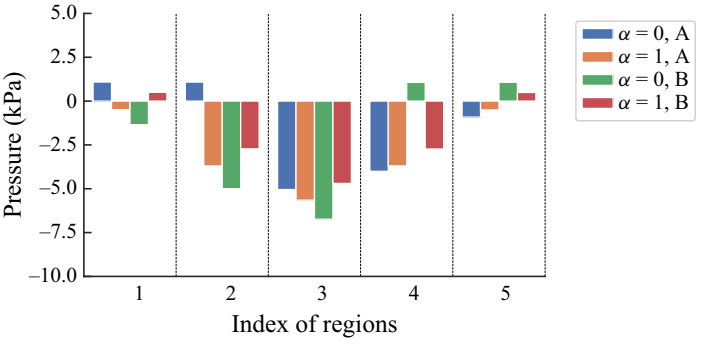

Figure 4. Exact solutions of the pressure distribution in each region: $U_H = 250\,\mathrm{km\,h^{-1}}$ and $R = 0.3$.

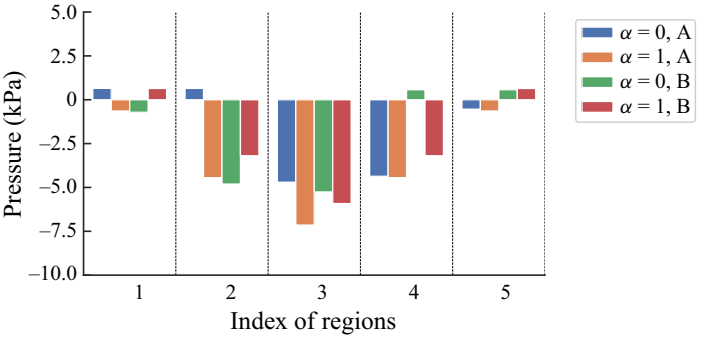

Figure 5. Exact solutions of the pressure distribution in each region: $U_H = 360\,\mathrm{km\,h^{-1}}$ and $R = 0.2$.

2.3. *Critical blockage ratio, R_c*

Figures 6 and 7 present the relationship between p_3, where the magnitude of the pressure reaches its maximum, and α. Here, '1st order equation' denotes the approximate solution, explained in § 3.1. For a small value of R (e.g. $R = 0.2$), $|p_3(\alpha = 0)|_{max} < |p_3(\alpha = 1)|_{max}$, whereas for a large value of R (e.g. $R = 0.3$), $|p_3(\alpha = 0)|_{max} > |p_3(\alpha = 1)|_{max}$. Here, $|p_3|_{max} = \max[|p_{3A}|, |p_{3B}|]$, and p_{3A} and p_{3B} are equal to p_3 for stages A and B, respectively.

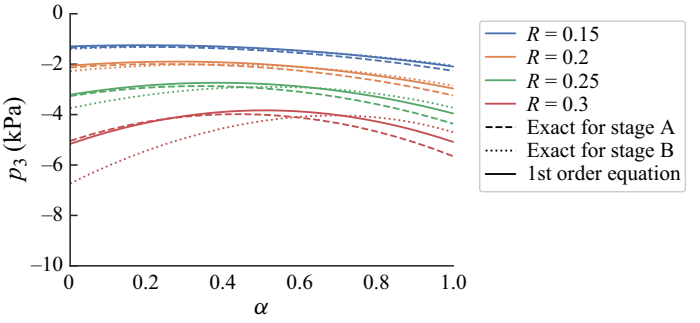

Figure 6. Relationship between p_3 and α ($U = 250\,\mathrm{km\,h^{-1}}$).

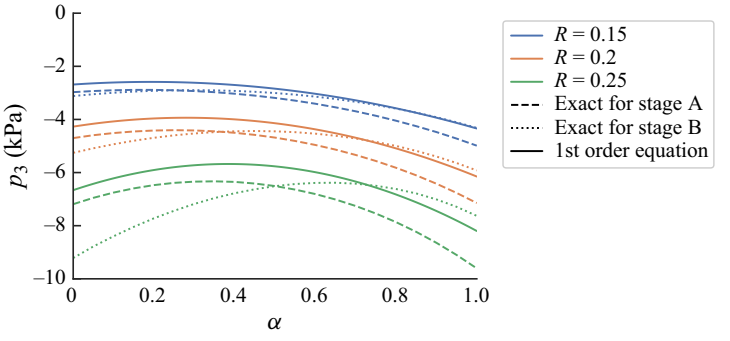

Figure 7. Relationship between p_3 and α ($U = 360\,\mathrm{km\,h^{-1}}$).

The critical blockage ratio R_c is defined as the blockage ratio R that satisfies the following condition:

$$|p_3\,(\alpha = 0)\,|_{max} = |p_3\,(\alpha = 1)\,|_{max}. \tag{2.9}$$

Figure 8 presents the exact solution of R_c, solved numerically. The value of R_c decreases with the train speed U_H. The value of R_c is 0.26 when $U_H = 320\,\mathrm{km\,h^{-1}}$. This indicates that the blockage ratio in conventional high-speed railway tunnels is smaller than R_c. Consequently, in cases involving mixed traffic with $U_H = 320\,\mathrm{km\,h^{-1}}$, the conservative worst-case scenario is two trains passing each other at identical speeds, that is, at $\alpha = 1$. Maglev trains ($R < 0.2$) also satisfy $R < R_c$ because $0.18 < R_c < 0.22$ for $500\,\mathrm{km\,h^{-1}} < U_H < 600\,\mathrm{km\,h^{-1}}$. Most railway tunnels (worldwide) are unlikely to allow the maximum value of R to exceed R_c; thus, the conservative estimation would be expected to be valid for these tunnels, considering only $\alpha = 1$.

3. Approximate equations

In this section, we introduce approximate equations of (2.1)–(2.8) for a detailed analysis of the results presented in § 2. Hara's analytical method (Hara 1961), originally used for analysing pressure waves generated by a train entering a tunnel with the assumption of $X_i \ll 1$, was applied to solve (2.1)–(2.8).

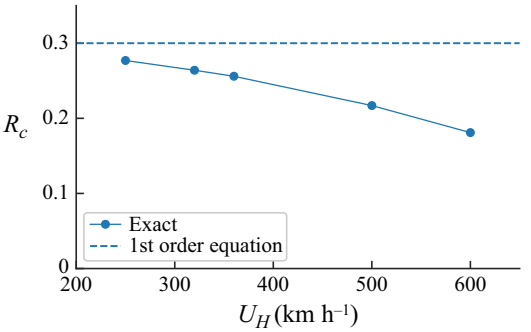

Figure 8. Critical blockage ratios at various speeds of the high-speed train.

3.1. *The Hara method*

Hara (Hara 1961) proposed a theoretical method to evaluate the pressure rise of the compression wave generated by a train entering a tunnel, where the terms of X^2 are only neglected among the second-order perturbations of the equations representing the compressible airflow, X^2, m^2 and $(\rho^* - 1)^2$. The results of model experiments and field tests show that the formula obtained in this manner effectively predicts the pressure rise. In the method, m^2 and $(\rho^* - 1)^2$ are expressed by X and the terms X^2 are neglected. When we neglect all the second-order perturbations, the system equations become those of linear acoustic theory (Howe 1998; Sugimoto & Ogawa 1998). In the Hara method, as the terms of the order of X^2 are neglected, the nonlinearity of pressure is ignored. However, it takes velocity nonlinearities and the velocity–pressure cross-term into account. Indeed, Miyachi (Miyachi 2019) showed that the Hara method considers the nonlinear source terms.

As $M \sim 0.3$ and $R \sim 0.2$ as described in § 2.1, we consider $M_H \ll 1$ and $R \ll 1$. The pressure rise of the compression wave generated by a train entering a tunnel is a weak shock given by $X \sim RM^2 \sim O[10^{-2}] \ll 1$. Therefore, it is regarded as $O[X_i^2 = R^2M^4] = O[10^{-4}]$, which can be neglected. Furthermore, because weak shocks satisfy the isentropic relation, $(\rho_i/\rho_0 - 1)^2 = O[X^2]$ can also be neglected. While $m \sim O[X = RM^2]$ for the air velocity accelerated by a weak shock, $m \sim O[M]$ for the air velocity around the train. Therefore, $m^2 \sim O[M^2] = O[10^{-1}]$ is considered.

The cross-terms between X and higher orders of M complicate the procedure. However, all terms of X are considered, even if the coefficient is a higher order of M (e.g. M^2X) in the original Hara method. Miyachi *et al.* (Miyachi *et al.* 2014) applied the Hara method to evaluate the pressure rise of pressure waves generated by a train passing a branch in a tunnel and showed that the results obtained by neglecting the cross-terms for simplicity are in agreement with the experimental results.

Each term of X_i is easily evaluated as $X_i \sim RM_H^2$, assuming the magnitude of the pressure beside a train travelling in a tunnel. This implies that $M_H \sim 0.3$, $R \sim 0.2$ and $X_i \sim RM_H^2$ for the train passing problem are the same as the tunnel entering problem. Therefore, the Hara method can be applied to (2.1)–(2.8). For simplicity, the cross-terms $M_HX_i \sim RM_H^3 \sim O[10^{-3}]$ and $M_H^2X_i \sim RM_H^4 \sim O[10^{-3}]$, respectively, are neglected in §§ 3.3 and 3.4. Therefore, the analysis in this study is based on the M_H expansion of X_i.

3.2. *Approximation of governing equations*

Here, we introduce an approximation of the governing equations for the approximate equations by neglecting $O[X_i^2]$. First, we evaluate the equations for each wave. Equations (2.1)–(2.3) yield the following equations:

$$\frac{\gamma(X_b - X_f)}{1 + \gamma X_f} = \frac{2\gamma}{\gamma + 1}\left(\left(\frac{m_f - M_s}{c_f/c_0}\right)^2 - 1\right), \tag{3.1}$$

$$\frac{\rho_b^*}{\rho_f^*} = \frac{m_f - M_s}{m_b - M_s} = \frac{(\gamma - 1)(1 + \gamma X_f) + (\gamma + 1)(1 + \gamma X_b)}{(\gamma + 1)(1 + \gamma X_f) + (\gamma - 1)(1 + \gamma X_b)}, \tag{3.2}$$

where (3.2) is the Rankine–Hugoniot equation.

Equation (3.2) gives

$$\frac{\rho_b^*}{\rho_f^*} = \frac{m_f - M_s}{m_b - M_s} = 1 + X_b - X_f + O[X^2] = \left(\frac{1/\gamma + X_b}{1/\gamma + X_f}\right)^{1/\gamma}. \tag{3.3}$$

As this result is well known, the isentropic relationship between the pressure in front of and behind a shock wave is obtained when $O[X_i^2]$ is neglected. Therefore, we can consider all the flow fields to be isentropic. Thus, we have

$$\rho_i^* = \frac{\rho_i}{\rho_0} = \left(\frac{1/\gamma + X_i}{1/\gamma}\right)^{1/\gamma} = 1 + X_i, \quad \text{for } i = 1, 2, 31, 32, 4, 5. \tag{3.4}$$

Therefore

$$M_s = m_f \mp \left(1 + \frac{\gamma + 1}{4}(X_b - X_f) + \frac{\gamma - 1}{2}X_f\right), \tag{3.5}$$

$$m_b - m_f = \mp(X_b - X_f), \tag{3.6}$$

where the positive sign denotes the propagation of the pressure wave in the positive x-direction.

From (3.4)–(3.6), by neglecting $O[X_i^2]$, we obtain the following for stage A:

$$\rho_1^* = 1 + X_1. \tag{3.7}$$

$$M_{s,I} = -\left(1 + \frac{\gamma + 1}{4}X_1\right), \tag{3.8}$$

$$m_1 = -X_1, \tag{3.9}$$

and for stage B:

$$\rho_1^* = 1 + X_1, \tag{3.10}$$

$$M_{s,III} = -\left(1 + \frac{\gamma + 1}{4}(X_1 + X_{A1})\right), \tag{3.11}$$

$$m_1 = -X_1, \tag{3.12}$$

where $X_{1A} = -m_{1A}$ is used (3.9).

Finally, we can use the same expression $m_1 = -X_1$ for stages A and B, although the values of X_1 for the two stages are different. Similarly, we also have the following for stages A and B:

$$m_5 = X_5. \tag{3.13}$$

Equations (2.8) and (3.4) yield $\rho_{31}^* = \rho_{32}^*$ when we neglect $O[X_i^2]$. Therefore, in this section, we consider the five regions, 1, 2, 3, 4 and 5, shown in figures 1 and 2. The equations for regions 2–4 are also simplified by neglecting $O[X_i^2]$. Substituting (3.4) into the continuity and Bernoulli equations (2.4) and (2.5) generates the following equations:

$$(1 + X_i)(m_i - M_{ref})(1 - R_i) = (1 + X_{i+1})(m_{i+1} - M_{ref})(1 - R_{i+1}), \tag{3.14}$$

$$X_i + \tfrac{1}{2}(m_i - M_{ref})^2 = X_{i+1} + \tfrac{1}{2}(m_{i+1} - M_{ref})^2. \tag{3.15}$$

From these results, the following equations are obtained after neglecting $O[X_i^2]$ for stage A:
Regions 0 and 1:

$$X_1 = -m_1. \tag{3.16}$$

Regions 1 and 2:

$$(1 + X_1)\,(m_1 - M_L) = (1 + X_2)\,(m_2 - M_L)\,(1 - R)\,, \tag{3.17}$$

$$X_1 + \tfrac{1}{2}\,(m_1 - M_L)^2 = X_2 + \tfrac{1}{2}\,(m_2 - M_L)^2\,. \tag{3.18}$$

Regions 2 and 3:

$$(1 + X_2)\,(m_2 + M_H)\,(1 - R) = (1 + X_3)\,(m_3 + M_H)\,(1 - 2R)\,, \tag{3.19}$$

$$X_2 + \tfrac{1}{2}\,(m_2 + M_H)^2 = X_3 + \tfrac{1}{2}\,(m_3 + M_H)^2\,. \tag{3.20}$$

Regions 3 and 4:

$$(1 + X_3)\,(m_3 - M_L)\,(1 - 2R) = (1 + X_4)\,(m_4 - M_L)\,(1 - R)\,, \tag{3.21}$$

$$X_3 + \tfrac{1}{2}\,(m_3 - M_L)^2 = X_4 + \tfrac{1}{2}\,(m_4 - M_L)^2\,. \tag{3.22}$$

Regions 4 and 5:

$$(1 + X_4)\,(m_4 + M_H)\,(1 - R) = (1 + X_5)\,(m_5 + M_H)\,, \tag{3.23}$$

$$X_4 + \tfrac{1}{2}\,(m_4 + M_H)^2 = X_5 + \tfrac{1}{2}\,(m_5 + M_H)^2\,. \tag{3.24}$$

Regions 5 and 0:

$$X_5 = m_5. \tag{3.25}$$

We obtain the equations for stage B by replacing M_L with $-M_H$ and M_H with $-M_L$ in (3.16)–(3.25). Although the speeds of the pressure waves differ for stages A and B ($c_{s,I} \neq c_{s,III}$), they do not explicitly appear in (3.16)–(3.25).

3.3. *First-order equations (equations of $O[M_H^2]$)*

The approximations of (3.16)–(3.25) when $O[X_i^2]$ and $O[M_H^3]$ are neglected for stage A are as follows (see Appendix B):

$$c_{p1} = \frac{R^2}{(1-R)(1-2R)}(1-\alpha^2) \geq 0, \tag{3.26}$$

$$c_{p5} = -c_{p1} \leq 0, \tag{3.27}$$

$$c_{p2} = \frac{R^2}{(1-R)(1-2R)} - \frac{R(2-(4-R)R)}{(1-R)^2(1-2R)}\alpha^2, \tag{3.28}$$

$$c_{p4} = \frac{R^2}{(1-R)(1-2R)}\alpha^2 - \frac{R(2-(4-R)R)}{(1-R)^2(1-2R)}, \tag{3.29}$$

$$c_{p3} = -\left[\frac{R}{1-R}(1+\alpha)^2 + \frac{R(1-R)}{(1-2R)^2}(1-\alpha)^2\right]. \tag{3.30}$$

As the relative errors of (3.26)–(3.30) denote the order of M_H (see Appendix B), these equations are first-order equations. Owing to the symmetry of the pressure fields between stages A and B, as shown in figures 1 and 2, replacing M_L with $-M_H$ and M_H with $-M_L$ in (3.26)–(3.30) yields the equations for stage B. Thus, we have shown that c_{p3} for stage B is the same as that for stage A. Similarly, c_{p1} for stage B is the same as c_{p5} for stage A.

From (3.26)–(3.30), we obtain the following pressure differences between two consecutive regions:

$$\Delta c_{p1} = \frac{X_1 - 0}{\frac{1}{2}M_H^2} = \frac{R^2}{(1-R)(1-2R)}(1-\alpha^2), \tag{3.31}$$

$$\Delta c_{p21} = \frac{\Delta X_{21}}{\frac{1}{2}M_H^2} = \frac{X_2 - X_1}{\frac{1}{2}M_H^2} = -\frac{R(2-R)}{(1-R)^2}\alpha^2, \tag{3.32}$$

$$\Delta c_{p32} = \frac{\Delta X_{32}}{\frac{1}{2}M_H^2} = \frac{X_3 - X_2}{\frac{1}{2}M_H^2} = -\frac{R(2-3R)}{(1-2R)^2}\left(1 - \frac{R}{1-R}\alpha\right)^2, \tag{3.33}$$

$$c_{p3} = \frac{X_3}{\frac{1}{2}M_H^2} = \Delta c_{p1} + \Delta c_{p21} + \Delta c_{p32}. \tag{3.34}$$

Figures 9–11 present the relationships between α and Δc_{p1}, Δc_{p21}, Δc_{p32} and c_{p3} for various values of R for stage A.

In (3.31), Δc_{p1} denotes the pressure rise of the pressure wave in front of train H. In (3.32), Δc_{p21} denotes the pressure drop beside train L (region 2) when it runs alone through incompressible air before passing train H (see Appendix C). In (3.33), Δc_{p32} denotes the pressure difference between regions 2 and 3 in an incompressible flow. Therefore, in the first-order equation, the pressure field around the two trains is the linear superposition of that of the incompressible flow and the pressure variation generated by the pressure waves. As $X_1 + X_5 = 0$, the impacts of the two pressure waves cancel out in region 3, and the two waves do not have any impact on this region. Moreover, in the

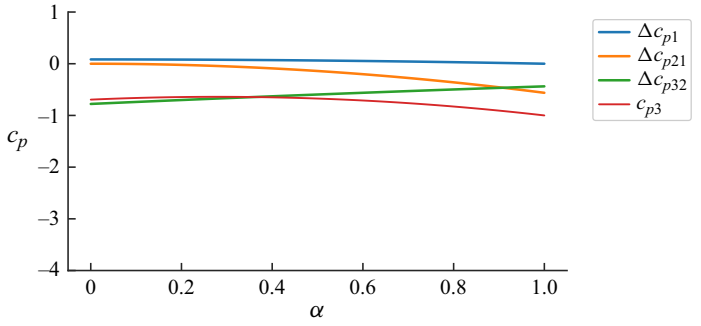

Figure 9. Relationships between pressure coefficients and α for $R = 0.2$ (first-order equations).

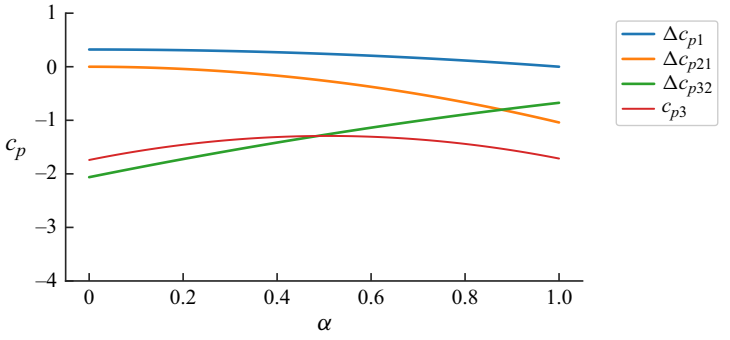

Figure 10. Relationships between pressure coefficients and α for $R = 0.3$ (first-order equations).

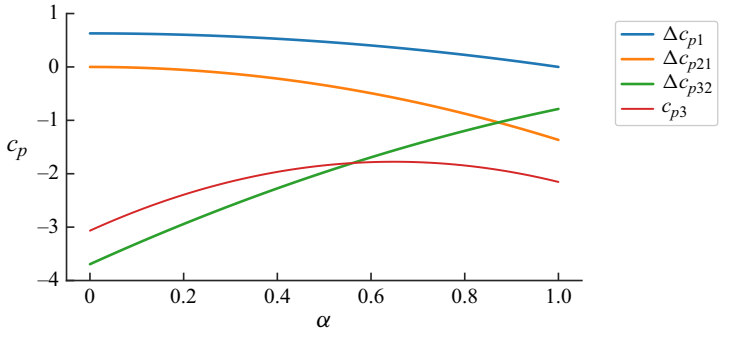

Figure 11. Relationships between pressure coefficients and α for $R = 0.35$ (first-order equations).

first order of R, we have $X_3 \sim X_2 + X_4 \sim -RM_H^2(1+\alpha^2)$. This means that the pressure between two passing trains is the approximate superposition of the pressure surrounding each train running alone.

The term ΔX_{21} is proportional to $\alpha^2 M_H^2$, which is the dynamic pressure of the low-speed train L. For $0 \le \alpha \le 1$ and $0 \le R \le 1/2$, (3.32) indicates that Δc_{p21} is a decreasing function of α and $\Delta c_{p21} \le 0$, implying that $|\Delta c_{p21}|$ is an increasing function of α (as shown in figures 9–11).

The term ΔX_{32} is proportional to $m_{2H}^2 = (1-(R/(1-R))\alpha)^2 M_H^2$, where $m_{2H} = (1-(R/(1-R))\alpha)M_H$ is the relative air velocity of region 2 in the coordinate system fixed on

train H. Here, $m_2 = -(R/(1-R))\alpha M_H$ is the speed of the airflow in region 2 induced by train L for incompressible flow. This implies that train L induces the airflow that follows train H with the speed $(R/(1-R))\alpha M_H$; this airflow that follows train H reduces the relative speed of train H and the magnitude of the pressure variation for the two trains passing each other. The effect of this reduction is more apparent as α increases; no following wind is observed for $\alpha = 0$. Equation (3.33) indicates that the vertex of Δc_{p32} is located at $\alpha = 1/R - 1 \geq 1$ for $0 \leq R \leq 1/2$. Therefore, for $0 \leq \alpha \leq 1$ and $0 \leq R \leq 1/2$, Δc_{p32} is an increasing function of α, and $\Delta c_{p32} < 0$. Thus, $|\Delta c_{p32}|$ is a decreasing function of α (as shown in figures 9–11).

The term X_1 is proportional to $(1-\alpha^2)M_H^2$, which is the difference in dynamic pressure between the two trains. Therefore, when the two trains pass each other at the same speed, $X_1 = 0$, that is, the compression wave generated by train H cancels out the expansion wave generated by train L in front of train H. For $0 \leq \alpha \leq 1$ and $0 \leq R \leq 1/2$, (3.31) indicates that Δc_{p1} is a decreasing function of α and $\Delta c_{p1} \geq 0$. Figures 9–11 indicate that this term is relatively small compared with Δc_{p21} and Δc_{p32}. For incompressible flow, $c_{p3} = \Delta c_{p21} + \Delta c_{p32} < 0$. However, the compressibility contributes to $|c_{p3}|$ through Δc_{p1}.

As Δc_{p21} is a decreasing function of α, $\Delta c_{p21}(\alpha = 0) > \Delta c_{p21}(\alpha = 1)$, whereas Δc_{p32} is an increasing function of α, and $\Delta c_{p32}(\alpha = 0) < \Delta c_{p32}(\alpha = 1)$. The magnitude of Δc_{p1} is relatively small compared with those of Δc_{p21} and Δc_{p32}. For a small value of R, as $\mathrm{d}\Delta c_{p21}/\mathrm{d}\alpha \sim -2R\alpha^2$ is the dominant term, c_{p3} is a decreasing function, whereas for a large value of R, as $\mathrm{d}\Delta c_{p32}/\mathrm{d}\alpha \sim 4R^2$ is also considerable, c_{p3} is an increasing function around $\alpha \sim 0$. The critical blockage ratio R_c, where the dominant term changes, satisfies the following equation:

$$c_{p3}\,(\alpha = 0) = c_{p3}\,(\alpha = 1)\,. \tag{3.35}$$

By solving the first-order equations (3.31)–(3.35), we have $R_c = (\sqrt{3}-1)/(2\sqrt{3}-1) = 0.297 \sim 0.3$. Figure 8 presents a comparison between the first-order and exact solutions of R_c. The first-order solution is constant as U_H changes, whereas the exact solution decreases with U_H. A coarse estimation of the maximum magnitude of the pressure induced by two trains passing through a tunnel is as follows:

$$|p_3\,(\alpha = 1)| = \left|-\frac{1}{2}\rho_0 U_H^2 \frac{4R}{1-R}\right|, \quad \text{for } R \leq 0.3, \tag{3.36}$$

$$|p_3\,(\alpha = 0)| = \left|-\frac{1}{2}\rho_0 U_H^2 \frac{R}{1-R}\left(1 + \left(\frac{1-R}{1-2R}\right)^2\right)\right|, \quad \text{for } R \geq 0.3. \tag{3.37}$$

3.4. *Second-order equations (equations of $O[M_H^3]$)*

The approximate equations of (3.16)–(3.25) when $O[X_i^2]$ and $O[M_H^4]$ are neglected for stage A are as follows (see Appendix B):

$$c_{p1A}^{(2)} = \frac{R^2}{(1-2R)\,(1-R)}(1-\alpha^2)$$

$$- \frac{R^2}{1-R}\frac{3}{4}M_H\left((1+\alpha)^3 + \frac{\frac{4}{3}R^2}{(1-R)(1-2R)^2}(1+\alpha)^2(1-\alpha) - \frac{1}{1-2R}(1+\alpha)(1-\alpha)^2\right), \tag{3.38}$$

$$c^{(2)}_{p5A} = -\frac{R^2}{(1-2R)(1-R)}(1-\alpha^2) - \frac{R^2}{1-R}\frac{3}{4}M_H\left((1+\alpha)^3 - \frac{\frac{4}{3}R^2}{(1-R)(1-2R)^2}(1+\alpha)^2(1-\alpha) - \frac{1}{1-2R}(1+\alpha)(1-\alpha)^2\right), \tag{3.39}$$

$$c^{(2)}_{p3A} = -\left[\frac{R}{1-R}(1+\alpha)^2 + \frac{(1-R)R}{(1-2R)^2}(1-\alpha)^2\right] - \frac{R^2}{1-R}\frac{3}{4}M_H(1+\alpha)^3 + \frac{R^2}{(1-2R)^3}\left(\frac{1}{1-R} - \frac{4}{3}R\right) \times \frac{3}{4}M_H(1+\alpha)(1-\alpha)^2, \tag{3.40}$$

$$c^{(2)}_{p2A} - c^{(2)}_{p1A} = -\frac{R(2-R)}{(1-R)^2}\alpha^2 - \frac{R^3(2-R)}{(1-2R)(1-R)^3}M_H\alpha(1-\alpha^2), \tag{3.41}$$

$$c^{(2)}_{p4A} - c^{(2)}_{p5A} = -\frac{R(2-R)}{(1-R)^2} + \frac{R^3(2-R)}{(1-2R)(1-R)^3}M_H(1-\alpha^2), \tag{3.42}$$

where $c^{(2)}_{piA}$ is the pressure coefficient in region i when considering $O[M_H^3]$ for stage A. As the relative errors of (3.38)–(3.42) denote the order of $O[M_H^2]$, these equations are second-order equations. Replacing M_L with $-M_H$ and M_H with $-M_L$ in these equations, we obtain the results for stage B, e.g.

$$c^{(2)}_{p3B} = -\left[\frac{R}{1-R}(1+\alpha)^2 + \frac{(1-R)R}{(1-2R)^2}(1-\alpha)^2\right] + \frac{R^2}{1-R}\frac{3}{4}M_H(1+\alpha)^3 - \frac{R^2}{(1-2R)^3}\left(\frac{1}{1-R} - \frac{4}{3}R\right)\frac{3}{4}M_H(1+\alpha)(1-\alpha)^2. \tag{3.43}$$

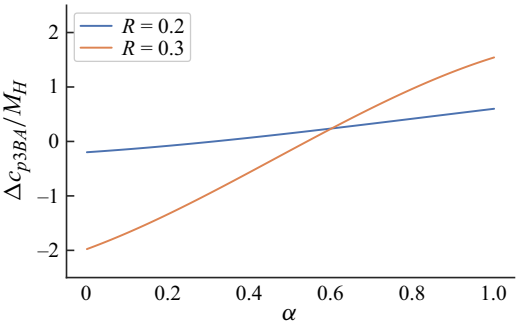

Figure 12. Pressure difference between stages A and B in region 3 (second-order equations).

The difference between the pressure in region 3 at stages A and B is as follows:

$$\Delta c^{(2)}_{p3BA} \equiv \Delta c^{(2)}_{p3B} - \Delta c^{(2)}_{p3A} = \left[\frac{1}{1-R}(1+\alpha)^3 - \frac{1}{(1-2R)^3}\left(\frac{1}{1-R} - \frac{4}{3}R\right)(1+\alpha)(1-\alpha)^2\right]\frac{3R^2M_H}{2}, \tag{3.44}$$

$$\Delta c^{(2)}_{p3BA}(\alpha = 0) = -\frac{R^2M_H}{2}\frac{2R\left(12\left(R-\frac{2}{3}\right)^2 + \frac{5}{3}\right)}{(1-R)(1-2R)^3}, \tag{3.45}$$

$$\Delta c^{(2)}_{p3BA}(\alpha = 1) = \frac{R^2M_H}{2}\frac{24}{1-R}. \tag{3.46}$$

Figure 12 presents the values of $\Delta c^{(2)}_{p3BA}/M_H$ for $R = 0.2$ and 0.3. For $0 \le R \le 1/2$, $\Delta c^{(2)}_{p3BA}$ is an increasing function of α; and here, $\Delta c^{(2)}_{p3BA}(\alpha = 0) < 0$ and $\Delta c^{(2)}_{p3BA}(\alpha = 1) > 0$. Therefore, $c^{(2)}_{p3B}(\alpha = 0) < c^{(2)}_{p3A}(\alpha = 0) < 0$ and $c^{(2)}_{p3A}(\alpha = 1) < c^{(2)}_{p3B}(\alpha = 1) < 0$. The maximum magnitude of the pressure as the two trains pass each other is observed in stages A and B for $\alpha = 1$ and 0, respectively, regardless of the value of R, as shown in figures 3–5.

Similarly, the pressure variations induced by pressure waves I and III, $\Delta c_{p,I}$ and $\Delta c_{p,III}$, respectively, are expressed as follows:

$$\Delta c^{(2)}_{p,\mathrm{I}} = c^{(2)}_{p1A} - 0 = \frac{R^2}{(1-2R)(1-R)}(1-\alpha^2)$$

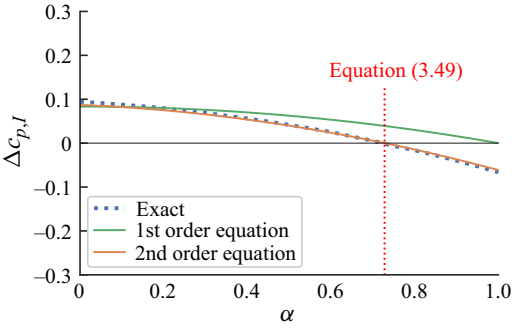

Figure 13. Pressure variations induced by pressure wave I: $U_H = 250\,\mathrm{km\,h^{-1}}$ and $R = 0.2$.

$$- \frac{R^2}{1-R}\frac{3}{4}M_H\left((1+\alpha)^3 + \frac{\frac{4}{3}R^2}{(1-R)(1-2R)^2}(1+\alpha)^2(1-\alpha) - \frac{1}{1-2R}(1+\alpha)(1-\alpha)^2\right), \tag{3.47}$$

$$\Delta c^{(2)}_{p,III} = \Delta c^{(2)}_{p1B} - c^{(2)}_{p1A} = -2\frac{R^2}{(1-2R)(1-R)}(1-\alpha^2) + \frac{R^2}{1-R}\frac{3}{2}M_H\left((1+\alpha)^3 - \frac{1}{1-2R}(1+\alpha)(1-\alpha)^2\right). \tag{3.48}$$

Figures 13–16 present the pressure variations induced by pressure waves I and III. In the first-order equations, pressure waves I and III are always compressive and expansive, respectively. In particular, for $\alpha = 1$, the pressure variations of these waves are zero. However, in the exact solutions or in the second-order equations, the variations are zero at $\alpha = \alpha_{cri} < 1$, where α_{cri} is the value of the zero pressure variation. As shown in the exact solutions in figures 13–16, α_{cri} is close to one. Solving each of $\Delta c^{(2)}_{p,I} = 0$ and $\Delta c^{(2)}_{p,III} = 0$ in the expanded form with $1 - \alpha$ and R yields the same solution as follows:

$$\alpha_{cri} = \frac{2 + 6R + 3(1+R)M}{2 + 6R + 9(1+R)M}. \tag{3.49}$$

For $\alpha > \alpha_{cri}$, pressure waves I and III are expansive and compressive, respectively, and *vice versa*. Figures 13–16 also show that the values of α_{cri} and the exact solutions are in good agreement.

Replacing M_H and M_L with M_L and M_H, respectively, in (3.47) and (3.48) yields $\Delta c_{p,II}$ and $\Delta c_{p,IV}$. Figures 17 and 18 show the pressure variation induced by pressure waves II and IV. Figures 17 and 18 indicate that pressure waves II and IV are always expansive and compressive, respectively. It is easily shown that $\Delta c_{p,I}(\alpha = 1) = \Delta c_{p,II}(\alpha = 1)$ and $\Delta c_{p,III}(\alpha = 1) = \Delta c_{p,IV}(\alpha = 1)$.

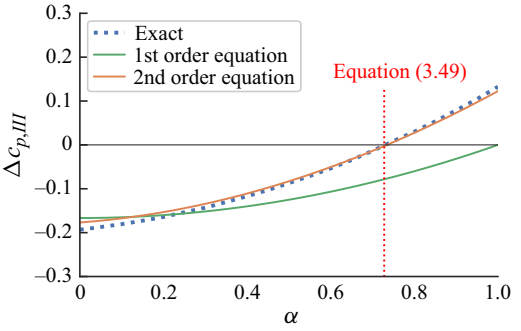

Figure 14. Pressure variations induced by pressure wave III: $U_H = 250\,\mathrm{km\,h^{-1}}$ and $R = 0.2$.

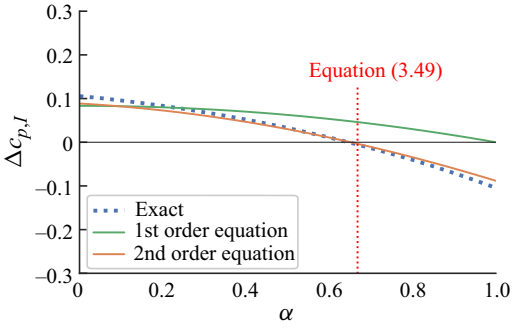

Figure 15. Pressure variations induced by pressure wave I: $U_H = 360\,\mathrm{km\,h^{-1}}$ and $R = 0.2$.

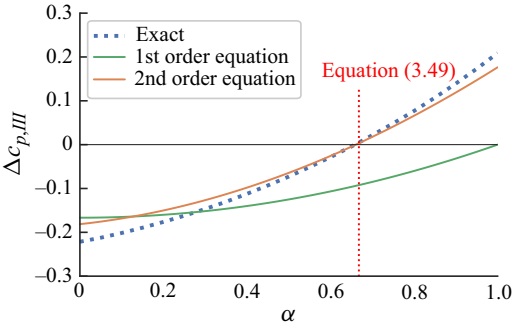

Figure 16. Pressure variations induced by pressure wave III: $U_H = 360\,\mathrm{km\,h^{-1}}$ and $R = 0.2$.

4. Discussion

In summary, we proposed three types of solutions for the pressure distribution generated when two trains pass each other in a tunnel: numerically exact solutions and solutions obtained using first- and second-order equations. It should be noted that the first-order equations are useful for rough estimations and qualitative understanding. The solutions proposed in this study enable the calculation of not only the maximum pressure magnitudes but also the time waveforms outside the trains, although they cannot provide the transient (or local) pressure variations around train noses and tails. The variation in the time waveforms is equivalent to the pressure difference between adjacent regions, such as Δc_{p21}.

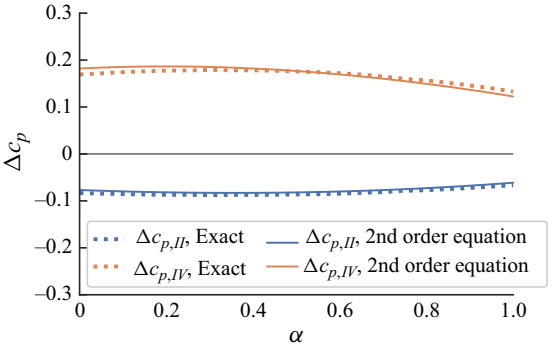

Figure 17. Pressure variations induced by pressure waves II and IV: $U_H = 250\,\mathrm{km\,h^{-1}}$ and $R = 0.2$.

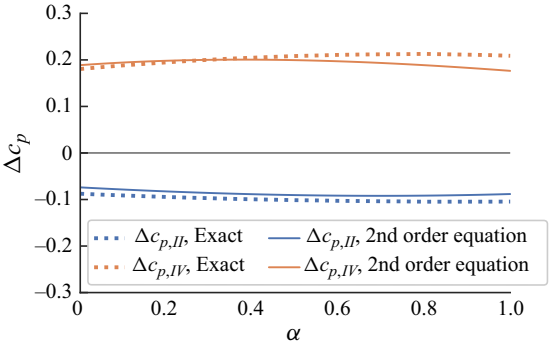

Figure 18. Pressure variations induced by pressure waves II and IV: $U_H = 360\,\mathrm{km\,h^{-1}}$ and $R = 0.2$.

In real-world scenarios, the pressure around two trains is superposed with that induced by pressure waves and friction. While employing 3-D CFD has proven effective for such a complicated problem, as reported in numerous studies (Fujii & Ogawa 1995; Hwang *et al.* 2001; Chu *et al.* 2014; Li *et al.* 2017; Lu *et al.* 2019; Qian *et al.* 2019), some limitations persist. For instance, Liu *et al.* (2018) noted that, owing to computational constraints, their calculations were restricted to cases involving short tunnels (less than one kilometre). Additionally, if all possible values of all parameters were considered, the application of 3-D CFD to scenarios involving two trains passing each other in a long tunnel, like the Seikan tunnel, would become challenging and impractical. Therefore, except for field tests, we must explore alternative approaches such as 1-D CFD, model experiments or theoretical analyses. Among these, conducting model experiments with two moving trains is difficult and theoretical solutions for two trains passing each other are yet to be derived. Therefore, 1-D CFD is the only practical method for addressing real-world scenarios. However, no means exist, other than field test data, to validate 1-D CFD analyses including two trains passing each other. This study not only facilitates the validation of 1-D CFD results but also extends the theoretical solutions (William-Louis & Tournier 2005) that simply aggregate amplitudes of pressure waves, pressure fields around trains and pressure induced by friction.

The main objective of this study is to estimate the negative pressure between two trains, X_3. When we simply sum the pressure surrounding the trains running at M_H and M_L assuming incompressible flow conditions, which are respectively equal to Δc_{p45} and Δc_{p21} as stated in § 3.3, the pressure $\Delta c_{p21} + \Delta c_{p45}$ is calculated using the first-order equation

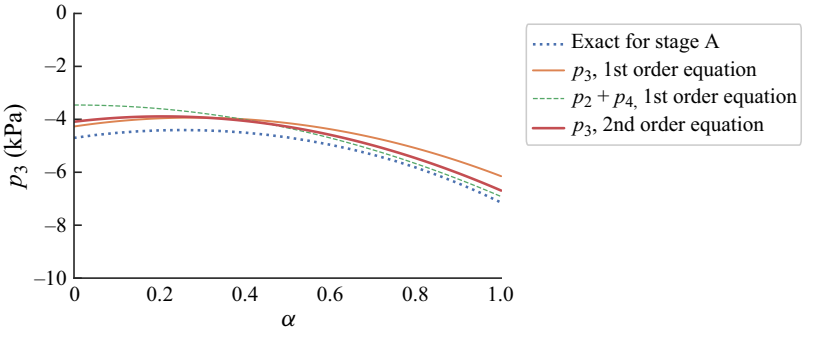

Figure 19. Comparison of p_3 and $p_2 + p_4$, stage A.

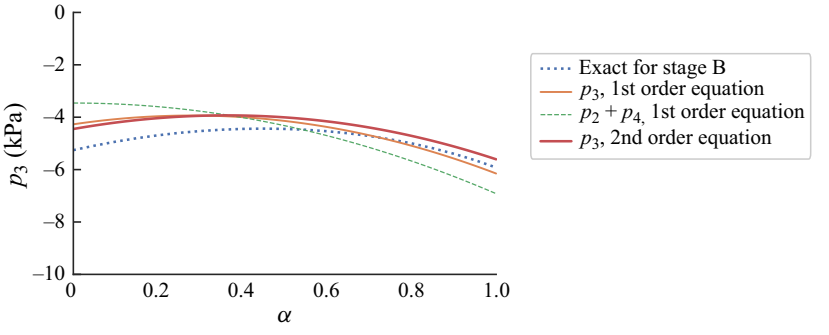

Figure 20. Comparison of p_3 and $p_2 + p_4$, stage B.

as follows:

$$\Delta c_{p21} + \Delta c_{p45} = \Delta c_{p21} + \Delta c_{p45} + \Delta c_{p1} + \Delta c_{p5} = c_{p2} + c_{p4} = -\frac{R\,(2-R)}{(1-R)^2}(1+\alpha^2), \tag{4.1}$$

because $\Delta c_{p1} + \Delta c_{p5} = 0$. As stated in § 3.3, in the first-order equation of R, $c_{p2} + c_{p4} \sim c_{p3}$. Figures 19 and 20 compare p_3 with $p_2 + p_4$. Here, $p_2 + p_4$ of the first-order equation is also a good approximation of the exact solutions. Although when compared with the exact solutions, the relative error of p_3 of the first-order equation varies with α and depends on the stage, that of the second-order equation is consistently small. Although an exact solution can be obtained in only a few seconds, the second-order equations are useful because of their simplicity. The first-order equation presents an effective understanding of the physical phenomena that prevail when the trains pass each other, as described in § 3.3.

The pressure waves that are generated by two trains passing each other, expressed as pressure waves I and II in this study, can cause micro-pressure waves when propagating to the ends of the tunnel. Howe (Howe 2000) presented a mathematical analysis of two trains passing each other at different speeds for stage A. In this analysis, the two trains were expressed as monopole source terms. Based on Howe's analysis, X_1 can be expressed as

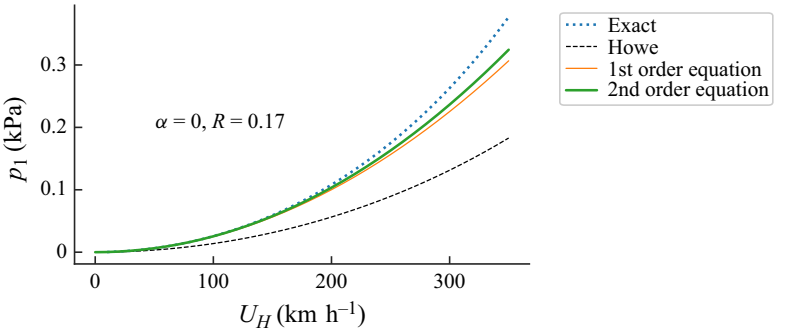

Figure 21. Relationship between p_1 and U_H for $\alpha = 0$ and $R = 0.17$.

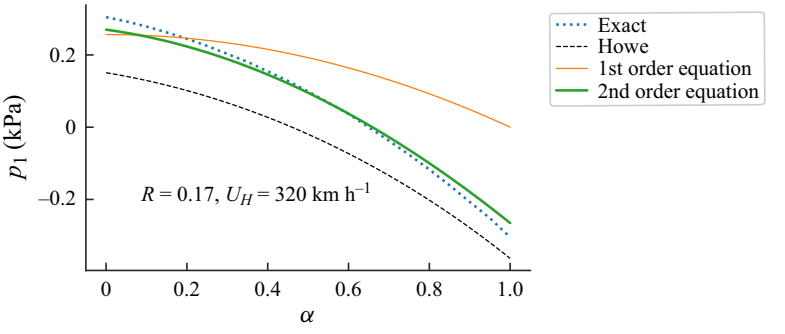

Figure 22. Relationship between p_1 and α for $U_H = 320\,\mathrm{km\,h^{-1}}$ and $R = 0.17$.

follows:

$$X_1 = (1+\alpha)\left[\frac{1}{(1+\alpha M_H)^2\,(1-M_H^2)} - \frac{\alpha}{(1-\alpha^2 M_H^2)\,(1-M_H)^2}\right] R^2 \frac{1}{2} M_H^2 \tag{4.2}$$

$$\sim R^2(1-\alpha^2)\frac{1}{2}M_H^2. \tag{4.3}$$

This formula corresponds with the main term of (3.26) for a low Mach number approximation. An analysis using monopole terms without nonlinear source terms neglects the higher terms of R (e.g. Howe 2000; Miyachi 2019), as explicitly observed in (3.38) and (4.3).

Figure 21 shows the relationship between p_1 and U_H for $\alpha = 0$ and $R = 0.17$, and figure 22 shows the relationship between p_1 and α for $U_H = 320\,\mathrm{km\,h^{-1}}$ and $R = 0.17$, where 'Howe' denotes the pressure obtained using (4.2). The parameters were set for a typical Japanese high-speed railway tunnel. These figures indicate that the results obtained using (3.38) are more accurate than those obtained using (3.26) and (4.2). The values of p_1 are negative for larger values of α, although $p_1 \geq 0$ for $0 \leq \alpha \leq 1$ in the first-order equation. This indicates that considering the high-order terms of R in (3.38) is important when analysing real-world high-speed railways. Although Howe's analysis can predict the waveforms of pressure waves, it is fairly complicated. In contrast, the analysis considered in this study is simple, although it can only be used to predict pressure magnitudes. Moreover, Howe's analysis can be modified by multiplying the ratio of (3.38) and (4.2).

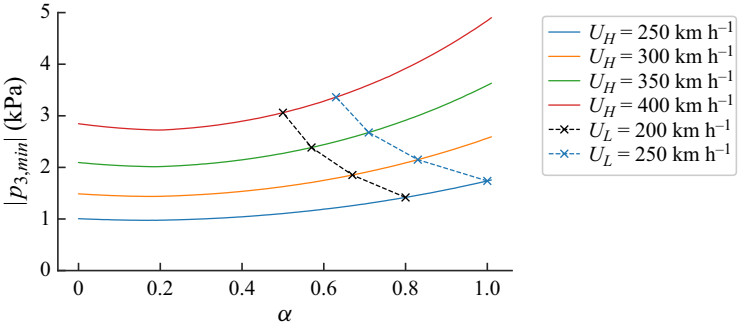

Figure 23. Relationship between the exact solution of $|p_{min}|$ and α when U_H or U_L is fixed for $R = 0.12$.

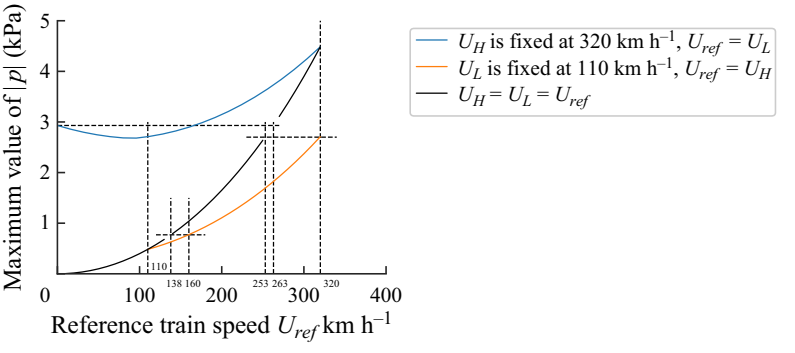

Figure 24. Relationship between U_{ref} and the maximum magnitude of the pressure for $R = 0.17$.

Figure 23 illustrates the relationship between the exact solution of $|p_{3,min}|$ and α when either U_H or U_L is fixed, where $p_{3,min}$ is the minimum value of p_3. When U_L is fixed, $|p_{3,min}|$ is a decreasing function of α. Conversely, as depicted in figure 23 and discussed in § 3.1, when U_H is fixed, $|p_{3,min}|$ is an increasing function of α for $R < R_c$. When U_L is fixed, the maximum value of $|p_{3,min}|$ decreases with α because U_H decreases.

Figure 24 depicts the maximum magnitude of the pressure when either U_H or U_L is fixed for $R = 0.17$. This figure presents three situations encountered in high-speed railway tunnels: (i) U_H is fixed at 320 km h^{-1} and $U_L = U_{ref}$ ($0 \le U_{ref} \le 320$ km h^{-1}); (ii) U_L is fixed at 110 km h^{-1} and $U_H = U_{ref}$ ($U_L = 110$ km h$^{-1} \le U_{ref} \le 320$ km h^{-1}); and (iii) $U_H = U_L = U_{ref}$ ($0 \le U_{ref} \le 320$ km h^{-1}).

In situation (i), because $R = 0.17 < R_c = 0.26$ for 320 km h^{-1}, the maximum magnitude of the pressure is lower at $U_L = 0$ than at $U_L = 320$ km h^{-1}. In situation (ii), the maximum magnitude of the pressure increases with U_H. The maximum magnitude of the pressure for the Seikan tunnel for $(U_L, U_H) = (110$ km h^{-1}, 160 km h$^{-1})$, which applies to the current operation, corresponds to that for $(U_L, U_H) = (138$ km h^{-1}, 138 km h$^{-1})$ in situation (iii). When U_H increases to 320 km h^{-1}, the maximum magnitude of the pressure for $(U_L, U_H) = (110$ km h^{-1}, 320 km h$^{-1})$ corresponds to that for $(U_L, U_H) = (253$ km h^{-1}, 253 km h$^{-1})$ in situation (iii). Therefore, increasing the speed limit in the Seikan tunnel to 320 km h^{-1} would require systems of freight cars to have approximately the same pressure air tightness and sealability as high-speed trains passing each other at 253 km h^{-1}; the current system does not have such air tightness and sealability. Moreover,

when $U_H = 320\,\mathrm{km\,h^{-1}}$ and $U_L \leq 110\,\mathrm{km\,h^{-1}}$, the worst case is the case for $(U_L, U_H) = (0, 320\,\mathrm{km\,h^{-1}})$ corresponding to that for $(U_L, U_H) = (263\,\mathrm{km\,h^{-1}}, 263\,\mathrm{km\,h^{-1}})$ in situation (iii). It should be noted that the maximum magnitude of the pressure for $(U_L, U_H) = (0, 320\,\mathrm{km\,h^{-1}})$ is greater than that for $(U_L, U_H) = (110, 320\,\mathrm{km\,h^{-1}})$. Therefore, requiring freight trains to remain stationary in the tunnel until the high-speed trains running at $320\,\mathrm{km\,h^{-1}}$ have passed is not necessarily the best solution.

5. Conclusion

In this study, we theoretically investigated asymptotic solutions of the pressure distribution in a tunnel when two trains pass each other running at different speeds. The following conclusions were drawn from the 1-D inviscid compressible steady airflow analysis.

(i) We proposed a method to obtain numerically exact solutions of the asymptotic pressure distribution around two trains passing each other in a tunnel while travelling at different speeds.

(ii) Theoretical formulas to predict the asymptotic pressure distribution when two trains pass each other at different speeds were obtained (first-order equations (3.26)–(3.30) and second-order equations (3.38)–(3.42)). The maximum values of the magnitudes of the pressures in the region occupied by the two trains were observed after nose–nose passing but before nose–tail passing, and after nose–tail passing but before tail–tail passing, when $\alpha = 1$ and 0, respectively.

(iii) When the speed of the high-speed train was fixed, the magnitude of the pressure was an increasing function of α for $R < R_c$, and the maximum magnitude of the pressure was obtained when the two trains passed each other at the same speed. However, for $R > R_c$, the maximum magnitude of the pressure was obtained when one train was stationary in the tunnel.

(iv) When the speed of the low-speed train was fixed, the maximum magnitude of the pressure was a decreasing function of α for $R < R_c$.

(v) As a coarse estimation, $R_c \sim 0.3$. When considering the effect of the speed of the train, R_c decreases with U_H. The exact values of R_c for $U_H = 320\,\mathrm{km\,h^{-1}}$ and $U_H = 600\,\mathrm{km\,h^{-1}}$ were 0.26 and 0.18, respectively.

(vi) Pressure waves I and III, generated in front of the high-speed train after nose–nose and nose–tail passing, respectively, were expansive and compressive for $\alpha > \alpha_c$, whereas pressure waves II and IV, generated in front of the low-speed train after nose–nose and nose–tail passing, respectively, were always expansive.

Therefore, for Japanese double-track tunnels, such as the mixed traffic Seikan tunnel, a conservative engineering estimation for two trains passing each other is obtained by assuming that both run at the same speed, with $\alpha = 1$ and $R < R_c$.

However, this study neglected the impacts of the pressure waves generated by a train entering or leaving a tunnel, boundary layer and friction, stagnation pressure around the nose and tail of a train, transient variation and three-dimensionality. The results of this study enable us to consider superposition of the pressure waves generated by two trains entering a tunnel and the pressure field around two trains passing each other.

Acknowledgements. The authors wish to thank Dr K. Kikuchi and Y. Araki of the Railway Technical Research Institute for helpful discussions and technical support, respectively.

Declaration of interests. The authors report no conflict of interest.

Author ORCIDs.
Tokuzo Miyachi https://orcid.org/0000-0002-6971-3549.

Appendix A. Application to other stages

In this appendix, we illustrate the application of the method to other stages in which the trains pass each other. Figure 25 shows stage A0, where pressure waves I and II propagate beside the trains. In this case, we can use (3.5) and (3.6) for pressure waves I and II and (3.14) and (3.15) for regions 0 and 2, I and 3, 3 and II and 4 and 0.

We have the same first-order equation of c_{p3} as (3.30) for stage A0. However, the second-order equation is obtained as follows:

$$\begin{aligned} c^{(2)}_{p3A0} = &-\left[\frac{R}{1-R}(1+\alpha)^2 + \frac{(1-R)R}{(1-2R)^2}(1-\alpha)^2\right] \\ &- \frac{R^2}{(1-R)^2}\frac{3}{4}M_H(1+\alpha)^3 + \frac{R^2}{(1-R)^2}\frac{3}{4}M_H \\ &\times\left(\frac{1}{1-2R} + \frac{\frac{2}{3}R(2-3R)}{(1-2R)^3}\right)(1+\alpha)(1-\alpha)^2. \end{aligned} \tag{A1}$$

Thus

$$|c^{(2)}_{p3A0}| - |c^{(2)}_{p3A}| \sim \tfrac{1}{4}M_H R^3[3(1+\alpha)^3 + (1+\alpha)(1-\alpha)^2]. \tag{A2}$$

This denotes that, before stage A, p_3 has a larger magnitude than (3.40), after which it approaches (3.40) asymptotically.

As described here, the values of p_3 slightly depend on the positions of pressure waves I and II. For simplicity, only the asymptotic state is analysed in this study.

Similarly, we can consider stage B0, which is the stage after nose–tail passing but before the waves move away from the trains, as shown in figure 26. In this stage, we need to consider six waves. Waves I and II are generated by nose–nose passing. Waves III-a–VI-b are newly generated by nose–tail passing. Waves III-a and IV-a propagate in the negative and positive x-directions, respectively. Thereafter, waves III-a–VI-b move away from the trains, and the stage asymptotically changes to stage B. Therefore, in stage B, we need to consider the six waves to be more exact than the treatment in § 2, as shown in figure 27. In this study, for simplicity, pressure wave III is considered as one wave consisting of two subwaves III-a and III-b, and wave IV is also considered as one wave. Although the wavelengths of waves III and IV are equal to the train length, when $X_i \ll 1$, this assumption does not affect the closed formula as all fields can be regarded as isentropic, and they negligibly affect the exact solutions.

Appendix B. Equations of $O[M_H^2]$ and $O[M_H^3]$

The equations of $O[M_H^2]$ presented in § 3.1 are introduced here. First, when using the continuity equations (3.17), (3.19), (3.21) and (3.23), and neglecting $O[X_i^2] = O[(RM_H^2)^2]$

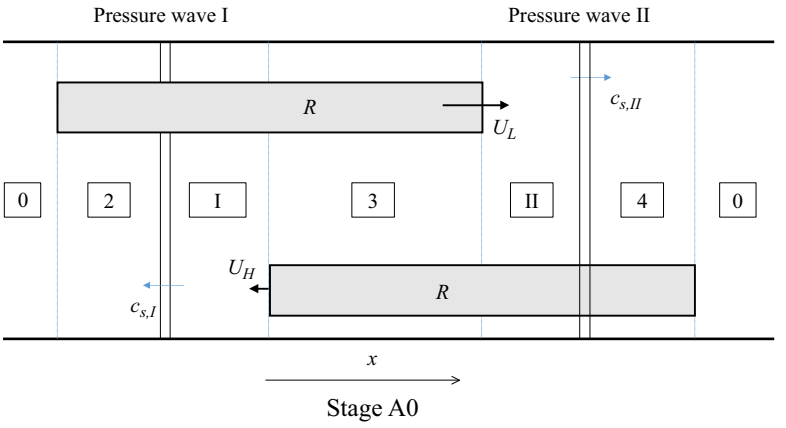

Figure 25. Schematic of two trains passing each other after nose–nose passing but before the waves move away from the trains.

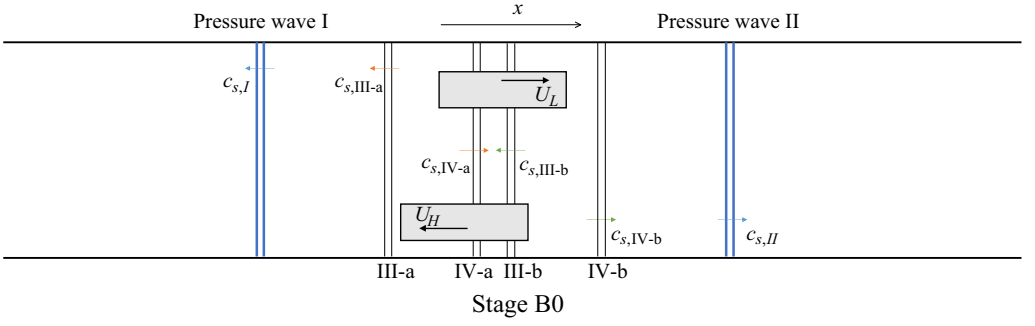

Figure 26. Schematic of two trains passing each other after nose–tail passing, stage B0.

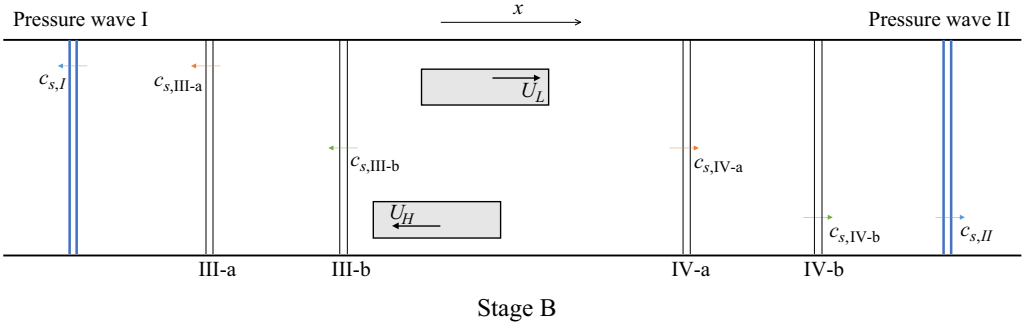

Figure 27. Schematic of two trains passing each other after nose–tail passing, stage B.

and $O[M_H X_i] = O[RM_H^3]$, we have

$$X_1 = -X_5. \tag{B1}$$

From (3.17)–(3.20), by neglecting $O[X_i^2] = O[(RM_H)^2]$ and $O[M_H X_i] = O[RM_H^3]$, we obtain

$$X_2 - X_1 = -\frac{R\,(2-R)}{(1-R)^2}\frac{1}{2}M_L^2, \tag{B2}$$

$$X_3 - X_2 = -\frac{R\,(2-3R)}{(1-2R)^2}\frac{1}{2}\left(-\frac{R}{1-R}M_L + M_H\right)^2. \tag{B3}$$

These results are the same as those obtained using the equations for incompressible flows. Similarly, using (3.21)–(3.24), we obtain

$$X_4 - X_5 = -\frac{R\,(2-R)}{(1-R)^2}\frac{1}{2}M_H^2, \tag{B4}$$

$$X_3 - X_4 = -\frac{R\,(2-3R)}{(1-2R)^2}\frac{1}{2}\left(-\frac{R}{1-R}M_H + M_L\right)^2. \tag{B5}$$

From (B2)–(B5), we have

$$X_5 - X_1 = -\frac{2R^2}{(1-2R)\,(1-R)}\frac{1}{2}(M_H^2 - M_L^2). \tag{B6}$$

Thus, we obtain the following equations in the expanded form of M_H:

$$\begin{aligned} X_1 &= \frac{R^2}{(1-2R)\,(1-R)}\frac{1}{2}(M_H^2 - M_L^2) + O[M_H^3] \\ &= \frac{R^2}{(1-2R)\,(1-R)}\frac{1}{2}(M_H^2 - M_L^2)\,(1 + O\,[M_H])\,, \end{aligned} \tag{B7}$$

$$c_{p1} = \frac{X_1}{\frac{1}{2}M_H^2} = \frac{R^2}{(1-2R)\,(1-R)}(1-\alpha^2) + O\,[M_H]\,. \tag{B8}$$

Finally, (3.26)–(3.30) and the solutions of the velocities are introduced below

$$m_1 = -X_1 = -m_5, \tag{B9}$$

$$m_2 = -\frac{R}{1-R}M_L - \frac{X_1}{1-R}, \tag{B10}$$

$$m_3 = -\frac{X_1}{1-2R} + \frac{R}{1-2R}\,(M_H - M_L)\,, \tag{B11}$$

$$m_4 = \frac{R}{1-R}M_H - \frac{X_1}{1-R}. \tag{B12}$$

When we consider the terms of the order of $O[M_H X_i] = O[M_H^3]$, for stage A, we have

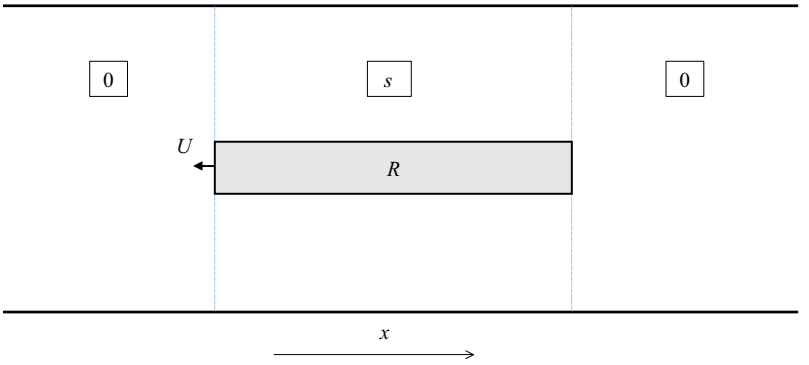

Figure 28. Schematic of one train running alone in a tunnel.

$$X_5 + X_1 = -\frac{6R^2}{1-R}\left(\frac{M_H + M_L}{2}\right)^3 + \frac{6R^2}{(1-R)(1-2R)}\left(\frac{M_H + M_L}{2}\right)(M_H - M_L)^2, \tag{B13}$$

$$X_3 - X_1 = -\frac{R(2-3R)}{(1-2R)^2}\frac{1}{2}\left(-\frac{R}{1-R}M_L + M_H\right)^2 - \frac{R(2-R)}{(1-R)^2}\frac{1}{2}M_L^2 - \frac{R(2-R)}{(1-R)^2}M_L X_1 + \frac{R(2-3R)}{(1-R)(1-2R)^2}\left(-\frac{R}{1-R}M_L + M_H\right)X_1, \tag{B14}$$

$$X_3 - X_5 = -\frac{R(2-R)}{(1-R)^2}\frac{1}{2}M_H^2 - \frac{R(2-3R)}{(1-2R)^2}\frac{1}{2}\left(\frac{R}{1-R}M_H - M_L\right)^2 - \frac{R(2-R)}{(1-R)^2}M_H X_5 + \frac{R(2-3R)}{(1-R)(1-2R)^2}\left(-\frac{R}{1-R}M_H + M_L\right)X_5. \tag{B15}$$

Equations (B13)–(B15) yield

$$X_1 = \frac{R^2}{(1-2R)(1-R)}\frac{1}{2}(M_H^2 - M_L^2) - \frac{R^2}{1-R}\frac{3}{8}(M_H + M_L) \times \left((M_H + M_L)^2 + \frac{\frac{4}{3}R^2}{(1-R)(1-2R)^2}(M_H^2 - M_L^2) - \frac{1}{1-2R}(M_H - M_L)^2\right). \tag{B16}$$

Appendix C. Pressure variation around a train running alone in tunnel

Figure 28 shows a schematic of one train running alone in a tunnel. From § 3.2, we have the following equations:

$$M = (1 + X_s)(m_s + M)(1 - R), \tag{C1}$$

$$\tfrac{1}{2}M^2 = X_s + \tfrac{1}{2}(m_s + M)^2. \tag{C2}$$

From these equations, by neglecting $O[X_s^2]$ and $O[M^2 X_s]$, we obtain

$$X_s = -\frac{1}{2} M^2 \frac{R\,(2-R)}{(1-R)^2}. \tag{C3}$$

This equation is the same as that for incompressible flow.

References

Baron, A., Mossi, M. & Sibilla, S. 2001 The alleviation of the aerodynamic drag and wave effects of high-speed trains in very long tunnels. *J. Wind Engng Ind. Aerodyn.* **89**, 365–401.

Chu, C.-R., Chien, S.-Y., Wang, C.-Y. & Wu, T.-R. 2014 Numerical simulation of two trains intersecting in a tunnel. *Tunn. Undergr. Space Technol.* **42**, 161–174.

Dundee Tunnel Research 2023 Thermotun – software. Available at: https://www.thermotun.com/thermotun/.

Fujii, K. & Ogawa, T. 1995 Aerodynamics of high speed trains passing by each other. *Comput. Fluids* **24** (8), 897–908.

Gawthorpe, R. 2000 Pressure effects in railway tunnels. Rail International. *Mon. Rev. IRCA/UIC*, **31**, 10–17.

Gilbert, T., Baker, C.J. & Quinn, A. 2013 Gusts caused by high-speed trains in confined spaces and tunnels. *J. Wind Engng Ind. Aerodyn.* **121**, 39–48.

Glöckle, H. & Pfretzschner, P. 1988 High speed tests with ICE V passing through tunnels, and the effect of sealed coaches on passenger comfort. In *Proceedings of 6th International Symposium on the Aerodynamics and Ventilation of Vehicle Tunnels*, p. A2. BHRA Group.

Hara, T. 1961 Aerodynamic force acting on a high speed train at the tunnel entrance. *Trans. Japan Soc. Mech. Engrs* **4**, 547–553.

Howe, M.S. 1998 The compression wave produced by a high-speed train entering a tunnel. *Proc. R. Soc. Lond.* A **454**, 1523–1534.

Howe, M.S. 2000 Pressure transients generated when high-speed trains pass in a tunnel . *IMA J. Appl. Maths* **65** (3), 315–334.

Howe, M.S., Iida, M., Maeda, T. & Sakuma, Y. 2006 Rapid calculation of the compression wave generated by a train entering a tunnel with a vented hood. *J. Sound Vib.* **297** (1), 267–292.

Hwang, J., Yoon, T., Lee, D. & Lee, S. 2001 Numerical study of unsteady flowfield around high speed trains passing by each other. *JSME Intl J.* B **44** (3), 451–464.

Kobayashi, M., Suzuki, Y., Akutsu, K. & Ozawa, S. 1998 Alleviating aural discomfort of passengers on shinkansen by controlling airflow rate in ventilation system. *JSME Intl J.* B **41** (4), 936–944.

Li, W.H., Liu, T.H., Zhang, J., Chen, Z.W., Chen, X.D. & Xie, T.Z. 2017 Aerodynamic study of two opposing moving trains in a tunnel based on different nose contours. *J. Appl. Fluid Mech.* **10** (5), 1375–1386.

Liu, T.-H., Chen, X.-D., Li, W.-H., Xie, T.-Z. & Chen, Z.-W. 2017 Field study on the interior pressure variations in high-speed trains passing through tunnels of different lengths. *J. Wind Engng Ind. Aerodyn.* **169**, 54–66.

Liu, K., Jing, L. & Ren, M. 2018 The characteristics of air wave induced by two high-speed trains passing by each other in a tunnel. *Adv. Mech. Engng* **10** (3), 1687814018766970.

Lu, Y., Zhang, D., Zheng, H., Lu, C., Chen, T., Zeng, J. & Wu, P. 2019 Analysis of the aerodynamic pressure effect on the fatigue strength of the carbody of high-speed trains passing by each other in a tunnel. *Proc. Inst. Mech. Engrs* F **233** (8), 783–801.

Miyachi, T. 2019 Non-linear acoustic analysis of the pressure rise of the compression wave generated by a train entering a tunnel. *J. Sound Vib.* **458**, 365–375.

Miyachi, T., Fukuda, T. & Saito, S. 2014 Model experiment and analysis of pressure waves emitted from portals of a tunnel with a branch. *J. Sound Vib.* **333**, 6156–6169.

Qian, W., Qi, T., Yi, H., Liang, X., Jin, Z., Lei, B., Li, Y. & Li, Z. 2019 Evaluation of structural fatigue properties of metro tunnel by model test under dynamic load of high-speed railway. *Tunn. Undergr. Space Technol.* **93**, 103099.

Railway Gazette International 2021 Seikan Services Speed up, p. 177. Railway Gazette International.

Saito, S., Iida, M. & Kajiyama, H. 2011 Numerical simulation of 1-D unsteady compressible flow in railway tunnels. *J. Environ. Engng* **6** (4), 723–738.

Sima, M. 2003 New unifying procedure for working with pressure tightness of rail passenger vehicles. In *Proceedings of the 11th International Symposium on Aerodynamics and Ventilation of Vehicle Tunnels*, pp. 743–757. BHR Group.

SUGIMOTO, N. & OGAWA, T. 1998 Acoustic analysis of the pressure field in a tunnel generated by entry of a train. *Proc. R. Soc.* A **454**, 2083–2112.

TOLLMIEN, W. 1927 Luftwiderstand und druckverlauf bei der fahrt von zögen in einem tunnel. *VDI-Zeitsch.* **71**/**6**, 199–203.

TSURU, M. 2021 Speed up in the Seikan tunnel (in Japanese). *Tetsudo J.* **55** (4), 9–17.

VARDY, A.E. 1976 The use of airshafts for the alleviation of pressure transients in railway tunnels. In *Proceedings of the Second International Symposium on the Aerodynamics and Ventilation of Vehicle Tunnels*, pp. 55–69. BHRA Group.

WILLIAM-LOUIS, M. & TOURNIER, C. 2005 A wave signature based method for the prediction of pressure transients in railway tunnels. *J. Wind Engng Ind. Aerodyn.* **93**, 521–531.

WOODS, W.A. & POPE, C.W. 1981 A generalised flow prediction method for the unsteady flow generated by a train in a single-track tunnel. *J. Wind Engng Ind. Aerodyn.* **7**, 331–360.

YAMAMOTO, A. 1974 Pressure variations, aerodynamic drag of train, and natural ventilation in Shinkansen type tunnel. *Q. Rep. RTRI* **15**, 207–213.

YANG, Q.-S., SONG, J.-H. & YANG, G.-W. 2016 A moving model rig with a scale ratio of 1/8 for high speed train aerodynamics. *J. Wind Engng Ind. Aerodyn.* **152**, 50–58.